www.czasopisma.pan.pl PAN www.journals.pan.pl
Opto-Electronics Review 27 (2019) 233–240

Contents lists available at ScienceDirect

Opto-Electronics Review

journal homepage: http://www.journals.elsevier.com/opto-electronics review

High sensitive and large dynamic range quasi-distributed sensing system based on slow-light π-phase-shifted fiber Bragg gratings

K.M. Dwivedi[a], T. Osuch[b,c,*], G. Trivedi[a]

[a] Dept. of Electronics and Electrical Engineering, IIT Guwahati, India
[b] Warsaw University of Technology, Institute of Electronic Systems, ul. Nowowiejska 15/19, 00-665 Warsaw, Poland
[c] National Institute of Telecommunications, ul. Szachowa 1, 04-894 Warsaw, Poland

ARTICLE INFO

Article history:
Received 16 April 2019
Received in revised form 4 June 2019
Accepted 6 June 2019
Available online 12 July 2019

Keywords:
π-FBG
Slow-light
Sensitivity
Quasi-distributed sensing
Transfer matrix method

ABSTRACT

In this paper, we theoretically analyze the slow-light π-phase-shifted fiber Bragg grating (π-FBG) and its applications for single and multipoint/quasi-distributed sensing. Coupled-mode theory (CMT) and transfer matrix method (TMM) are used to establish the numerical modeling of slow-light π-FBG. The impact of slow-light FBG parameters, such as grating length (L), index change (Δn), and loss coefficient (α) on the spectral properties of π-FBG along with strain and thermal sensitivities are presented. Simulation results show that for the optimum grating parameters L = 50 mm, $\Delta n = 1.5\times10^{-4}$, and α = 0.10 m^{-1}, the proposed slow-light π-FBG is characterized with a peak transmissivity of 0.424, the maximum delay of 31.95 ns, strain sensitivity of 8.380 $\mu\varepsilon^{-1}$, and temperature sensitivity of 91.064 $^{\circ}C^{-1}$. The strain and temperature sensitivity of proposed slow-light π-FBG is the highest as compared to the slow-light sensitivity of apodized FBGs reported in the literature. The proposed grating have the overall full-width at half maximum (FWHM) of 0.2245 nm, and the FWHM of the Bragg wavelength peak transmissivity is of 0.0798 pm. The optimized slow-light π-FBG is used for quasi-distributed sensing applications. For the five-stage strain quasi-distributed sensing network, a high strain dynamic range of value 1469 $\mu\varepsilon$ is obtained for sensors wavelength spacing as small as 2 nm. In the case of temperature of quasi-distributed sensing network, the obtained dynamic range is of 133 °C. For measurement system with a sufficiently wide spectral range, the π-FBGs wavelength grid can be broadened which results in substantial increase of dynamic range of the system.

1. Introduction

During the past few decades, optical fiber sensors (OFSs) have attracted increasing attention in various practical applications [1,2]. They show unique advantages over electronics counterparts, such as passive, low loss, high sensitivity, immunity towards electromagnetic interferences/radio frequency interferences (EMI/RFI), chemically inert, and lightweight. OFSs can be developed to sense single point, multipoint/quasi-distributed, and fully distributed measurements [3]. A multipoint/quasi-distributed OFS network is realized by multiplexing of point sensors in a series along a single fiber. Quasi-distributed OFS networks are capable to monitor the entire structure. Fiber Bragg Grating (FBG) based quasi-distributed OFS network shows higher resolution than distributed OFS [3]. Moreover, FBG has some additional inherent properties, such as wavelength encoded measurement, excellent multiplexing capability, small size, easily embedded into the systems, and large dynamic range sensing. Furthermore, the spectral and delay responses of FBG can be easily tuned by varying the index-change of the grating, such as apodization [4], tilting [5], chirp [6], tapering [7], etc. Therefore, they are extensively adapted in many real field applications. These days, FBG based quasi-distributed sensing networks are preferred for monitoring health of structures [8,9] and perimeter security [10].

Several types of multiplexing techniques have been proposed for FBG based multipoint/quasi-distributed sensing networks, including time division multiplexing (TDM) [11], wavelength division multiplexing (WDM) [12], a combination of TDM and WDM [13], space division multiplexing (SPD) [14], etc. Among these multiplexing techniques, WDM based quasi-distributed sensing

* Corresponding author at: Warsaw University of Technology, Institute of Electronic Systems, Nowowiejska 15/19, 00-665 Warsaw, Poland.
E-mail addresses: krishna.dwivedi@iitg.ac.in (K.M. Dwivedi), T.Osuch@elka.pw.edu.pl (T. Osuch).

https://doi.org/10.1016/j.opelre.2019.06.004
1230-3402/

interrogation scheme is the most preferable because of its high speed. However, the number of FBG sensors in WDM networks is limited by source spectrum range. The number of sensors in the WDM network can be increased by reducing the FWHM and side-lobes of reflected spectra of multiplexed FBG sensors. In recent years, several apodization profiles have been proposed to optimize the optical characteristics, such as FWHM, maximum side-lobes (MSL), average side-lobes, side-lobes suppression ratio (SLSR), etc., of FBG for dense WDM (DWDM) based quasi-distributed strain and temperature sensing networks [15–17].

This paper presents the single and quasi-distributed strain and temperature sensing based on slow-light π-FBG. Slow-light FBG sensors are well-known for enhanced sensitivity and better resolution than conventional FBG-based sensors. The slow-light in FBG can be achieved by providing the high refractive index change or/and long grating length. In the conventional FBGs, slow light was not observed due to the grating have either a weak index change or the grating length was too small or not optimized for the weak index change [18]. Recently, high index change fiber Bragg grating based slow-light has gained huge popularity in the optical communication and in sensing applications [18,19]. The index change for a slow-light FBG sensor is 10–30 times stronger than the normal FBG sensors. Slow-light in uniform, apodized, and tilted Bragg gratings and their application in sensing systems have been studied theoretically and experimentally in Refs. [9,20–23]. The experimental results for micro displacement sensing show that slow-light FBG has 13 times higher sensitivity and resolution than normal FBG [20]. A remarkable strain resolution of 30 fε/$\sqrt{}$Hz at 30 kHz and strain sensitivity of 3.8 $\mu\varepsilon^{-1}$ is reported in Ref. [21]. The strain resolution is an order of magnitude lower than conventional FBG based sensors. More recently, Arora *et al.* proposed a slow-light FBG temperature sensor having temperature resolution of 0.3 m°C /$\sqrt{}$Hz which is nearly 30 times lower than conventional FBG [24]. However, the proposed slow-light grating shows the very low temperature sensitivity of 5.2 °C^{-1} (calculated) due to the low transmissivity peak. It is well-known that the sensitivity of slow-light FBG is proportional to the product of delay and transmissivity of FBG [25]. The delay and sensitivity spectra of uniform and apodized FBGs have more than one peak. Moreover, maximum sensitivity peak of apodized FBG is also very unpredictable [18]. Therefore, these gratings are not suitable for quasi-distributed sensing applications.

A π-FBG exhibits single and high delay peak in the delay spectra which can be utilized for multipoint/quasi-distributed sensing networks. However, the transmissivity spectrum of π-FBG have multiple side-lobes which reduces the maximum dynamic range. Recently, we have proposed a new symmetrical apodization profile for sensing and communication applications [26]. The same apodization profile is used to mitigate the side-lobes of π-FBG too. Other apodization profile may also be used; however, a strong apodization must be avoided because it reduces the slow-light peak sensitivity. The detailed studies of the optical (transmissivity and delay) and sensing characteristics of slow-light π-FBG is presented in this manuscript. The optical and sensing characteristics of slow-light π-FBG are optimized with respect to slow-light grating parameters [grating length (L), index change (Δn), and loss coefficient (α)]. The optimum grating parameters for which the π-FBG shows maximum delay and sensitivity are obtained as L =50 mm, Δn = 1.5×10^{-4}, and α =0.10 m^{-1}. The proposed slow-light π-FBG is characterized with peak transmissivity of 0.424, maximum delay of 31.95 ns, strain sensitivity of 8.380 $\mu\varepsilon^{-1}$, and temperature sensitivity of 91.064 °C^{-1}. The highest slow-light strain and temperature sensitivity of 3.8 $\mu\varepsilon^{-1}$ [21] and 22.1 °C^{-1} [25], respectively, are reported in the literature for the apodized FBGs. As compared to the slow-light sensitivity of apodized FBGs, strain and temperature sensitivity of proposed π-FBG is the highest. The proposed grating have the overall full-width at half maximum (FWHM) of 0.2245 nm and the FWHM of the Bragg wavelength peak transmissivity is of 0.0798 pm. The optimized slow-light π-FBG is used for quasi-distributed sensing applications. A high strain dynamic range of value 1469 $\mu\varepsilon$ is obtained for five-stage strain sensing network. For the five-stage temperature sensing network, the obtained dynamic range is of 133 °C. The additional advantage of slow-light π-FBG in quasi-distributed sensing networks over the conventional apodized FBG sensing networks is that slow-light peaks are free from the side-lobes. Therefore, slow-light sensing networks do not require a guard band between the two sensors when the external perturbation is applied [16,17].

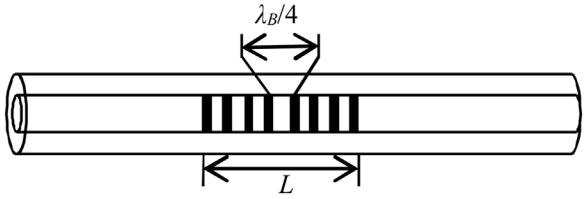

Fig. 1. Schematic diagram of π-FBG.

The rest of the paper is organized as follows: numerical model of slow-light π-FBG and its sensitivity are presented in Section 2; Section 3 presents results and discussion; In Section 4 optimized π-FBG slow-light is used for quasi-distributed sensing; and Section 5 presents the conclusion.

2. Numerical model of the slow-light π-FBG

The variation of effective refractive index of fiber along the grating length L is given as [27]:

$$n_{eff}(z) = n_{eff} + \overline{\delta n}(1 + \nu f(z)\cos[\frac{2\pi}{\Lambda}z + \phi(z)]),\ 0 < z < L, \tag{1}$$

where n_{eff} is the effective refractive index of a fiber in the absence of grating; $\overline{\delta n}$ denotes the averaged index change for a single grating period; ν stands for the fringe visibility of index change; $f(z)$ is the apodization profile; Λ is the period of grating and $\phi(z)$ is the grating chirp. The presence of a periodic variation of refractive index change in FBG creates a band of finite reflection bandwidth in the frequency space, where light is not allowed to propagate [18]. A discrete phase shift of quarter-wave (π-phase) in the index change at the middle point of grating length opens a band gap in the reflection bandwidth and produces a narrow transmission band. Therefore, a π-FBG can be easily visualized as a Fabry-Perot (FP) cavity formed by two similar FBGs having cavity length of $\lambda_B/4$, where λ_B is the Bragg wavelength of FBG as shown in Fig. 1. The light trapped in this cavity accumulates π phase per round excursion. Moreover, the cavity length of this FP cavity is so tiny that it supports a single and sharp transmission peak at Bragg wavelength. The modeling of slow-light π-FBG has been performed using coupled-mode theory and transfer matrix method.

The CMT describing slow-light grating, however, requires modification due to the loss coefficient. The modified couple-mode differential equations (CMDE) for slow-light grating are given as [27,28]:

$$\frac{dR_f}{dz} + \frac{\alpha}{2}R_f = i\hat{\sigma}R_f(z) + i\kappa R_b(z) \tag{2}$$

$$\frac{dR_b}{dz} + \frac{\alpha}{2}R_b = -i\hat{\sigma}R_b(z) - i\kappa^* R_f(z), \tag{3}$$

where $R_f(z) = A_f(z)\exp\left(i\delta z - \phi/2\right)$ and $R_b(z) = A_b(z)\exp\left(i\delta z - \phi/2\right)$ are the forward and backward propagating modes having slowly varying amplitudes of A_f and A_b, respectively; $\delta = \beta - \beta_B$ is the detuning from the phase matching condition; $\kappa = \pi\nu f(z)\overline{\delta n}/\lambda$ is the AC coupling coefficient for fundamental core mode; the apodization profile is $f(z) = J_0\left(\cos\left(3z/L\right)\right)^8\left(\cos\left(2z/L-1\right)\right)^4$, where J_0 is the ordinary Bessel function of 1st kind of order 0 [26]; α stands for the loss coefficient and $\hat{\sigma} = \delta + \sigma - \frac{1}{2}\frac{d\phi}{dz}$ denotes the general DC self-coupling coefficient. For slow-light gratings general DC self-coupling coefficient is defined as:

$$\begin{aligned}\overline{\sigma} &= \hat{\sigma} + i\frac{\alpha}{2} = \delta + \sigma - \frac{1}{2}\frac{d\phi}{dz} + i\frac{\alpha}{2} \\ &= 2\pi n_{eff}\left(\frac{1}{\lambda} - \frac{1}{\lambda_B}\right) + \frac{2\pi}{\lambda}\overline{\delta n} - \frac{1}{2}\frac{d\phi}{dz} + i\frac{\alpha}{2},\end{aligned} \tag{4}$$

where σ is the DC coupling coefficient, $\lambda_B = 2n_{eff}\Lambda$ is Bragg wavelength and $\frac{1}{2}\frac{d\phi}{dz}$ denotes chirped of the grating period. For uniform grating $\frac{1}{2}\frac{d\phi}{dz} = 0$.

The slow-light optical characteristics of non-uniform FBG, such as reflectivity, transmissivity, delay, etc., can be easily and accurately obtained by solving the slow-light CMDE Eq. (2) and Eq. (3) using transfer matrix method [29]. In this approach, grating length L is divided into N uniform sections of length $\delta l\left(\delta l \gg \Lambda\right)$ and constant values of κ and σ are assigned to each uniform section. The transfer matrix of i^{th} section is described as [27]:

$$T_i = \begin{bmatrix} \cosh\left(\Omega_i\delta l_i\right) - i\frac{\overline{\sigma}}{\Omega_i}\sinh\left(\Omega_i\delta l_i\right) & -i\frac{\kappa_i}{\Omega_i}\sinh\left(\Omega_i\delta l_i\right) \\ i\frac{\kappa_i}{\Omega_i}\sinh\left(\Omega_i\delta l_i\right) & \cosh\left(\Omega_i\delta l_i\right) + i\frac{\overline{\sigma}}{\Omega_i}\sinh\left(\Omega_i\delta l_i\right) \end{bmatrix}, \tag{5}$$

where $\Omega_i = \sqrt{\kappa_i^2 - \overline{\sigma}_i^2}$.

The response of π-FBG is given by:

$$\begin{aligned}\begin{bmatrix} R_{fN} \\ R_{bN} \end{bmatrix} &= [T_N][T_{N-1}]\cdots[T_{ps}]\cdots[T_2][T_1]\begin{bmatrix} R_{f0} \\ R_{b0} \end{bmatrix}, \\ &= \left(\prod_{i=1}^{N} T_i\right)\begin{bmatrix} R_{f0} \\ R_{b0} \end{bmatrix}\end{aligned} \tag{6}$$

where R_{f0} and R_{b0} are the input forward and backward field amplitudes, respectively, and R_{fN} and R_{bN} correspond to the output field amplitudes. T_{ps} is the phase-shift matrix and can be given as [27]:

$$T_{ps} = \begin{bmatrix} e^{-i\phi/2} & 0 \\ 0 & e^{i\phi/2} \end{bmatrix}, \tag{7}$$

where ϕ is the shift in the phase of grating and defined as $\phi/2 = 2\pi n_{eff}\Delta z/\lambda$, Δz stands for the separation between two grating sections. Applying the appropriate boundary conditions ($R_{f0} = 1$ and $R_{bN} = 0$) in Eq. (6), the reflection and transmission coefficients of the grating are calculated as:

$$\rho = \frac{T_{21}}{T_{22}} \tag{8}$$

$$t = \frac{1}{T_{11}}. \tag{9}$$

The transmitted/reflected light will experience some delay in the cavity due to the multiple reflections. The delay time of transmitted light is given as [27]:

$$\tau_t = \frac{d\theta_t}{d\omega} = -\frac{\lambda^2}{2\pi c}\frac{d\theta_t}{d\lambda}, \tag{10}$$

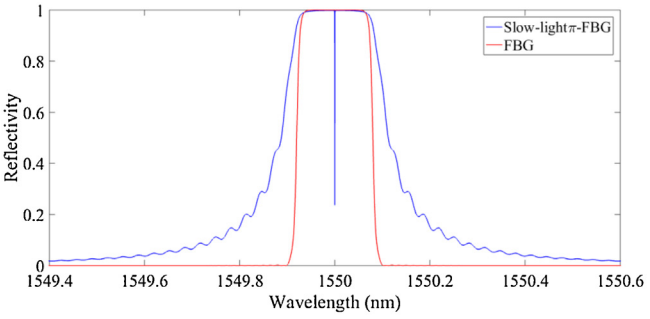

(a)

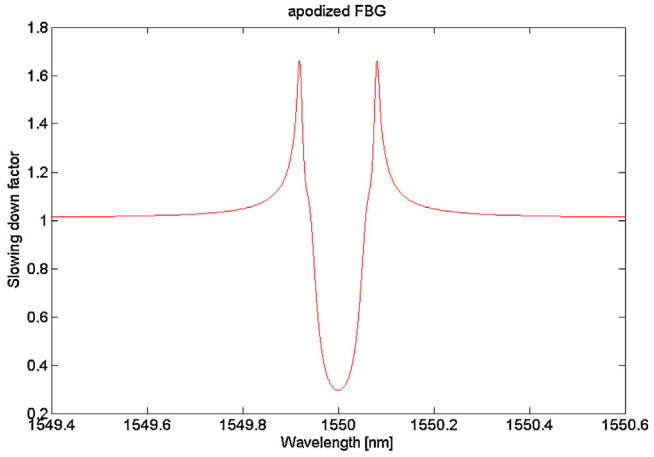

(b)

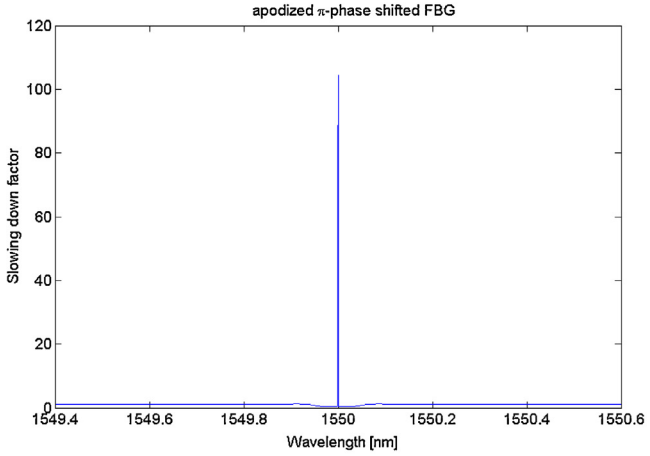

(c)

Fig. 2. (a) Reflectivity spectra of slow-light π-FBG and conventional FBG (b) slowing down factor for conventional FBG (c) slowing down factor for slow-light π-FBG.

where θ_t stands for the phase of transmitted light,ω denotes the optical frequency, and c is the speed of light in vacuum. The cavity length of FP interferometer made by π-FBG is small enough to support a single and sharp transmission and delay peaks at Bragg wavelength. Figure 2 shows the reflectivity spectra and slowing down factor of slow-light π-FBG and conventional FBG. A slowing down factor is defined as the ratio of the average group velocity to group velocity of light in the medium [30]. As shown in the Fig. 2(b)

and Fig. 2(c) the slowing down factor for π-FBG is much greater than the conventional FBG. Therefore, a much slower light is obtained in π-FBG as compare to the conventional FBG.

The sensitivity of slow-light FBG sensor is given as [25]:

$$S_x(\lambda) = \frac{dT(\lambda)}{dx} = \frac{dT(\lambda)}{d\lambda}\frac{d\lambda}{dx}, \tag{11}$$

where x is the external perturbation, $T(\lambda)$ is the transmissivity of FBG as a function of λ. According to Lorentzian slow-light resonance, the maximum value of $dT(\lambda)/d\lambda$ is $3\sqrt{3}T_0/4\Delta\lambda$ at wavelength $\lambda = \lambda_B \pm \Delta\lambda\sqrt{3}/6$, where T_0 is the peak transmission at Bragg wavelength, and Δλ is FWHM of the Lorentzian [25]. The value of Δλ in the terms of transmitted delay time τ_t is given as $\Delta\lambda = \lambda_B^2/\pi c\tau_t$. Thus, Eq. (11) can be written as:

$$S_x(\lambda) = \frac{4.08c\tau_t T_0}{\lambda_B^2}\frac{d\lambda}{dx} \tag{12}$$

FBGs are inherently sensitive to strain and temperature. FBG measures all other possible physical parameters as a derivative of strain or temperature. The shift in Bragg wavelength of FBG due to the change in strain and temperature is given as:

$$d\lambda = (K_\varepsilon \Delta\varepsilon + K_T \Delta T)\lambda_B, \tag{13}$$

where $K_\varepsilon \approx 0.78 \times 10^{-6}\varepsilon^{-1}$ and $K_T \approx 8.6 \times 10^{-6}{}^{\circ}C^{-1}$ are strain and thermal sensitivity coefficients, respectively. Thus, at zero temperature change, from Eqs. (12) and (13), slow-light strain sensitivity is obtained as

$$S_\varepsilon(\lambda) = 3.182 \times 10^{-6}\frac{c\tau_t T_0}{\lambda_B} \tag{14}$$

Similarly, slow-light temperature sensitivity at zero strain change is obtained as:

$$S_T(\lambda) = 3.508 \times 10^{-5}\frac{c\tau_t T_0}{\lambda_B}. \tag{15}$$

It can be seen from Eqs. (14) and (15), that slow-light sensitivity depends on the product of delay and peak transmissivity at Bragg wavelength which is relevant "figure of merit (FoM)" of slow-light FBG sensors.

3. Results and discussion

In this section, first we optimize the peak transmissivity, delay, and sensitivity of π-FBG as the function of slow-light grating parameters (grating length, index change, and loss-coefficient). For analyzing π-FBG, peak transmissivity, delay, and sensitivity are the values at Bragg wavelength, λ_B. The variation of peak transmissivity and delay of π-FBG with respect to grating length and index change are shown in Fig. 3 and Fig. 4, respectively at zero loss coefficients. The peak transmissivity gradually decreases as the grating length or index-change increases (in Fig. 3 and Fig. 4). It happens

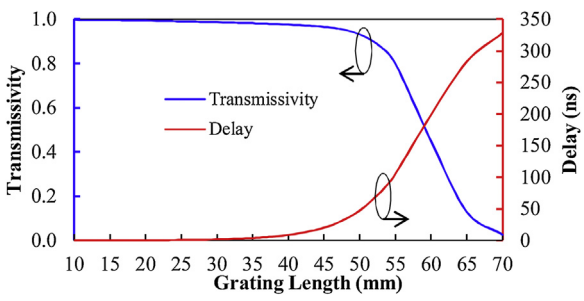

Fig. 3. Transmissivity and group delay *vs.* grating length for fixed $\Delta n = 1.5 \times 10^{-4}$ and $\alpha = 0$.

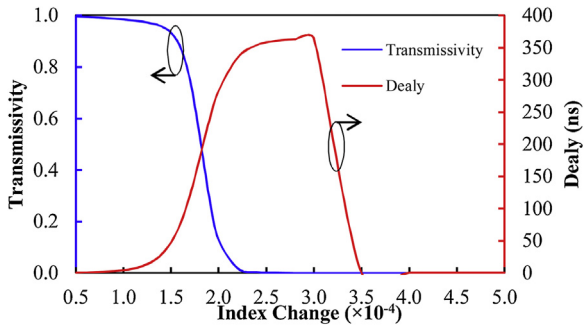

Fig. 4. Transmissivity and group delay *vs.* index change for fixed $L = 50$ mm and $\alpha = 0$.

because an increase in grating length or index change makes grating stronger and as a result the diffraction efficiency of the grating increases. As shown in Fig. 3, for a fixed index change of 1.5×10^{-4}, with the increase in the grating length up to 70 mm, peak transmissivity of π-FBG is trended to zero. This is because the grating becomes stronger and most of the light power reflected back at the initial length of the grating. Similar result is observed in Fig. 4, for fixed grating length 50 mm, the peak transmissivity trended to zero for index change greater than 2.4×10^{-4}.

The delay of slow-light π-FBG shows a different pattern from the transmissivity. As the grating length increases the delay is also increased gradually. It happens because as the grating length increases the reflectivity of FP mirrors made by π-FBG increases and light trap in the cavity travels back and forth several times and experiencing enhanced delay. A similar result is also obtained for the index change up to 2.2×10^{-4} as shown in Fig. 4. Further increment in index-change results in a very slow increment in delay. It is due to the very slow increment in the refractivity of FP mirrors, hence light trap in cavity experiences nearly the same time delay. The delay decreases sharply after index change of 3.0×10^{-4} (in Fig. 4). This is because grating becomes very strong and light power in the cavity reduced to zero.

It is known that the loss coefficient plays a crucial role in slow-light measurements. The value of loss coefficient is dependent upon many factors including grating fabrication technology and index change [19]. The effect of loss coefficients on transmissivity and delay are shown in Fig. 5. The values of loss coefficients are taken from literature [18–21,23–25]. As the loss coefficient increases, the transmissivity and delay decrease. With the increment in the loss coefficient transmissivity is trended to zero for the short grating length. For the large loss coefficients, delay is first increased for the certain length of grating and become constant. It happens because as the grating length increase the reflectivity of FP mirrors is increased which increases the quality factor of the cavity. Further increase in grating length, the propagation loss becomes dominated on cavity loss; therefore, constant delay is observed.

The sensitivity is directly proportional to the FoM of slow-light FBG. For the highest sensitivity, the FoM must be optimum with respect to slow-light grating parameters. The effects of slow-light grating parameters, grating length L, index change Δn, and loss coefficient α on FoM are plotted in Fig. 6, Fig. 7 and Fig. 8, respectively. For the zero loss coefficient, as the grating length increases up to 60 mm (in Fig. 6) and index-change up to 1.8×10^{-4} (in Fig. 7), FoM increases gradually to the highest value. It is because for the given range of grating length or index-change, delay is increased sharply than the decrement in transmissivity as shown in Fig. 3 and Fig. 4. Further increment in grating length or index-change, FoM of π-FBG is decreased sharply because in these range transmissivity and delay both are decreased.

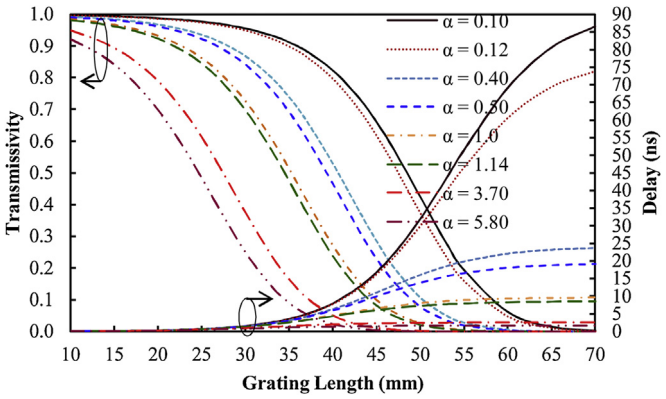

Fig. 5. Transmissivity and delay *vs.* grating length with different loss coefficients for fixed $\Delta n = 1.5 \times 10^{-4}$.

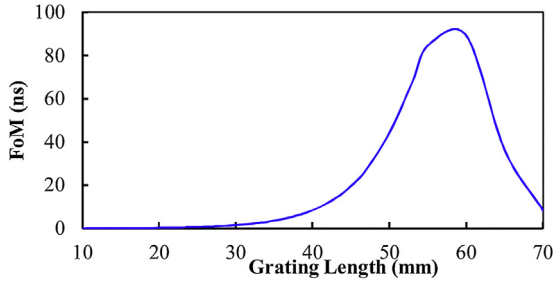

Fig. 6. FoM *vs.* grating length for $\Delta n = 1.5 \times 10^{-4}$ and $\alpha = 0$.

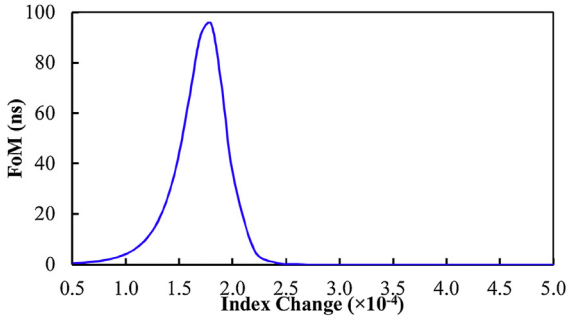

Fig. 7. FoM *vs.* index change for L =50 mm and $\alpha = 0$.

Figure 8 shows the dependency of FoM on grating length for the different loss coefficients. As the loss coefficient increases the peak of FoM decreases and shifts toward the shorter grating length. It happens because an increase in loss coefficient reduces the transmissivity, as well as delay. In addition to this, as the loss coefficient increases the peak of delay is shifted towards the shorter grating length.

For the highest sensitivity FoM must be the highest. Above results show that for the highest FoM loss coefficients must be as low as possible. The lowest loss coefficient reported in the literature is of 0.10 m^{-1} for the index change of 1×10^{-3} [25]. However, the same loss coefficient is used in this manuscript to optimize the grating length for low index change of 1.5×10^{-4}. Figure 8 shows that for the fixed index change of 1.5×10^{-4} the highest FoM of 13.5361 ns is obtained at the grating length of 50 mm.

The transmissivity, delay, strain and temperature sensitivity of optimized π-FBG (L =50 mm, $\Delta n = 1.5 \times 10^{-4}$, and $\alpha = 0.10\ m^{-1}$) are shown in Fig. 9 for the illustration. The proposed π-FBG is characterized with peak transmissivity of 0.424, maximum delay of 31.95 ns, strain sensitivity of 8.380 $\mu\varepsilon^{-1}$, and temperature sensitivity of 91.064 °C^{-1}. The proposed grating has the overall FWHM of 0.2245 nm and the FWHM of the Bragg wavelength peak transmissivity is of 0.0798 pm.

4. Quasi-distributed sensing system

The optimized slow-light π-FBG is utilized for quasi-distributed sensing networks. Figure 10 shows the transmissivity and strain sensitivity spectra of the five-stage quasi-distributed strain-sensing network without any external perturbation. Each sensor has assigned a unique wavelength of λ_{B1} = 1546.12 nm, λ_{B2} = 1548.11 nm, λ_{B3} = 1550.12 nm, λ_{B4} = 1552.12 nm, and λ_{B5} = 1554.13 nm, respectively. The channel spacing between two adjacent wavelengths is of 2 nm [15,16]. Figure 11 shows the transmissivity and strain sensitivity spectra of the same quasi-distributed strain-sensing network, but exerted with the strain to the third sensor (λ_{B3} = 1550.12 nm), while other sensors are kept free from external perturbation. The FWHM of proposed slow-light FBG is of 0.2245 nm. Therefore, the maximum allowable red shift in a wavelength is of 1.7755 nm. For the given red shift, the maximum allowable strain is obtained as 1469 $\mu\varepsilon$. The transmissivity spectrum is very complicated, while the strain sensitivity spectrum shows two sharp and distinct sensitivity peaks. However, the two sensitivity peaks are not equal, as shown in Fig. 11. It is due to the amplitude modulation which increases the sharpness of transmissivity of 3rd sensor; a result in higher sensitive peak is observed for the 3rd sensor [25]. Moreover, the slow-light sensitive peaks are free from side-lobes which show an additional advantage over conventional apodized FBG sensing networks [15–17]. Therefore, no guard band needed between the two sensors when the external perturbation is applied [16,17]. A similar result can also be obtained for the five-stage quasi-distributed temperature sensing networks. The maximum temperature dynamic range is found to be 133 °C. Furthermore, if we had a measurement system with a sufficiently wide spectral range, the FBGs grid can be broadened which results in increase of dynamic range of the system.

5. Conclusions

Slow-light FBG sensors show the high sensitivity and better resolution as compared to conventional FBG sensors. In this paper, we have studied slow-light π-FBG for single and quasi-

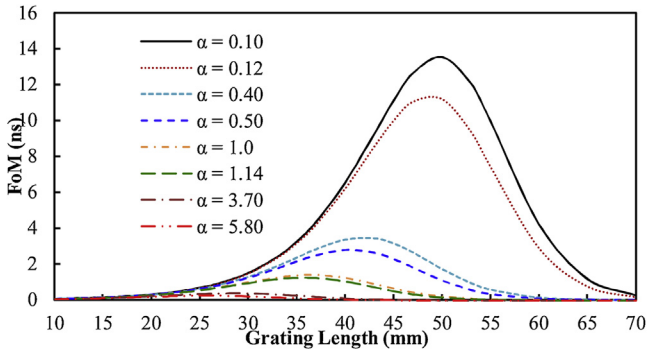

Fig. 8. FoM *vs.* grating length with different loss coefficients for fixed $\Delta n = 1.5 \times 10^{-4}$.

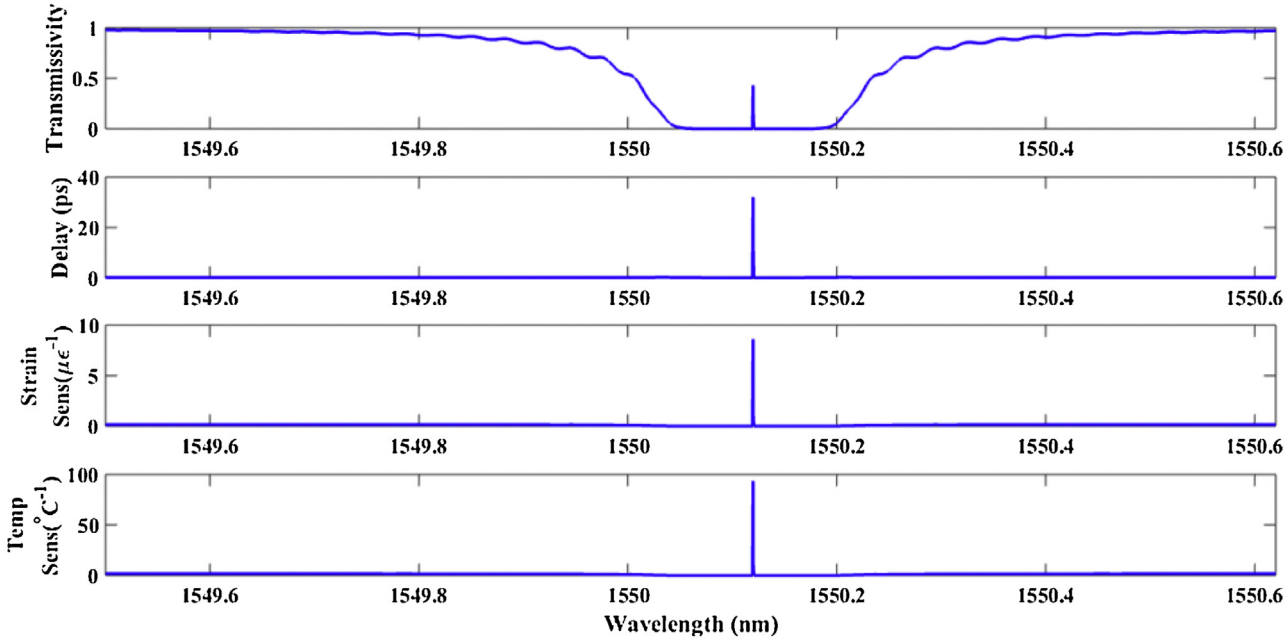

Fig. 9. Optical and sensing spectra of optimized slow-light π-FBG.

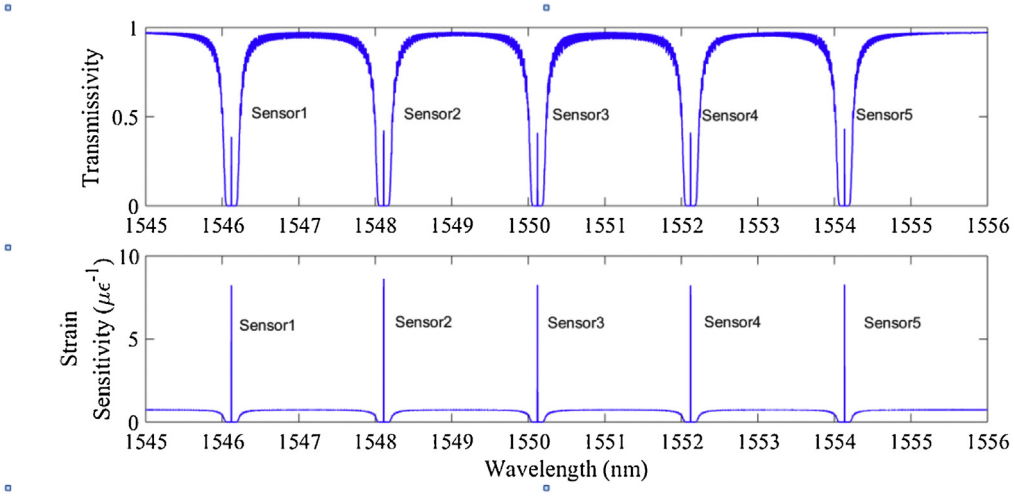

Fig. 10. Five-stage quasi-distributed strain sensing applications of optimized slow-light π-FBG.

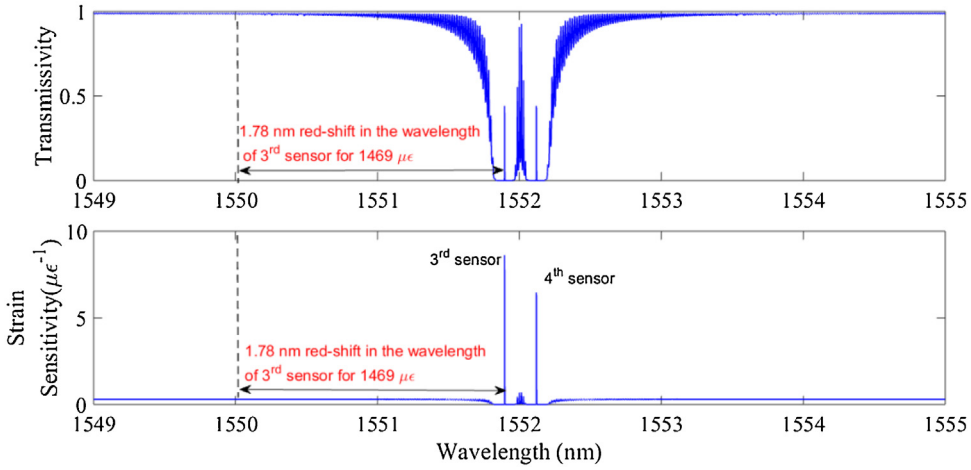

Fig. 11. Quasi-distributed sensing of optimized slow-light π-FBG with applied strain of 1469 με to the third sensor only.

distributed sensing applications. Slow-light grating parameters, such as grating length L, index change Δn, and loss coefficient α, are optimized for the sensing applications. For the optimum grating parameters, L=50 mm, $\Delta n = 1.5\times10^{-4}$, and $\alpha = 0.10\,m^{-1}$, the proposed slow-light π-FBG is characterized with peak transmissivity of 0.424, maximum delay of 31.95 ns, strain sensitivity of 8.380 $\mu\varepsilon^{-1}$, and temperature sensitivity of 91.064 $^{\circ}C^{-1}$. The highest slow-light strain and temperature sensitivity of 3.8 $\mu\varepsilon^{-1}$ [21] and 22.1 $^{\circ}C^{-1}$ [25], respectively, are reported in the literature for the apodized FBGs. As compared to the slow-light sensitivity of apodized FBGs, strain and temperature sensitivity of proposed π-FBG is the highest. The proposed grating have the overall FWHM of 0.2245 nm and the FWHM of the Bragg wavelength peak transmissivity is of 0.0798 pm. The optimized slow-light π-FBG is used for quasi-distributed sensing applications. A high strain dynamic range of the value of 1469 $\mu\varepsilon$ is obtained for a five-stage strain sensing network. For the five-stage temperature sensing network, the obtained dynamic range is of 133 °C. The additional advantage of a slow-light π-FBG in quasi-distributed sensing networks over the conventional apodized FBG sensing networks is that slow-light peaks are free from the side-lobes. Therefore, slow-light sensing networks do not require a guard band between the two sensors when the external perturbation is applied.

References

[1] B. Lee, Review of the present status of optical fiber sensors, Opt. Fiber Technol. 9 (2003) 57–79.
[2] C.K.Y. Leung, K.T. Wan, D. Inaudi, X. Bao, W. Habel, Z. Zhou, J. Ou, M. Ghandehari, H.C. Wu, M. Imai, Review: optical fiber sensors for civil engineering applications, Mater. Struct. 48 (4) (2015) 871–906.
[3] J.M. López-Higuera, L.R. Cobo, A.Q. Incera, A. Cobo, Fiber optic sensors in structural health monitoring, J. Lightwave Technol. 29 (4) (2011) 587–608.
[4] T. Osuch, Z. Jaroszewicz, Numerical analysis of apodized fiber Bragg gratings formation using phase mask with variable diffraction efficiency, Opt. Commun. 284 (2011) 567–572.
[5] E. Elzahaby, I. Kandas, M. Aly, K. Mahmoud, Sensitivity improvement of reflective tilted FBGs, Appl. Opt. 55 (12) (2016) 3306–3312.
[6] K. Ennser, N. Zervas, R. Laming, Optimization of apodized linearly chirped fiber gratings for optical communications, IEEE J. Sel. Top. Quantum Electron. 34 (1998) 770–778.
[7] T. Osuch, K. Jędrzejewski, L. Lewandowski, W. Jasiewicz, Shaping the spectral characteristics of fiber Bragg gratings written in optical fiber taper using phase mask method, Photon. Lett. Poland 4 (2012) 128–130.
[8] M. Majumder, T.K. Gangopadhyay, A.K. Chakraborty, K. Dasgupta, D.K. Bhattacharya, Fibre Bragg gratings in structural health monitoring—present status and applications, Sens. Actuators A Phys. 147 (2008) 150–164.
[9] Y. Dai, Y. Liu, J. Leng, G. Deng, A. Asundi, A novel time-division multiplexing fiber Bragg grating sensor interrogator for structural health monitoring, Opt. Lasers Eng. 47 (2009) 1028–1033.
[10] H. Wui, Y. Qian, W. Zhang, H. Li, X. Xie, Intelligent detection and identification in fiber-optical perimeter intrusion monitoring system based on the FBG sensor network, Photon. Sens. 5 (2015) 365–375.
[11] Y. Wang, J. Gong, B. Dong, D.Y. Wang, T.J. Shillig, A. Wang, A large serial time-division multiplexed fiber Bragg grating sensor network, J. Lightwave Technol. 30 (2012) 2751–2756.
[12] Y. Yu, L. Lui, H. Tam, W. Chung, Fiber-laser-based wavelength division multiplexed fiber Bragg grating sensor system, IEEE Photon. Technol. Lett. 13 (2001) 702–704.
[13] Z. Luo, H. Wen, H. Guo, M. Yang, A time- and wavelength-division multiplexing sensor network with ultra-weak fiber Bragg gratings, Opt. Exp. 21 (2013) 22799–22807.
[14] K. Stępień, M. Slowikowski, T. Tenderenda, M. Murawski, M. Szymanski, L. Szostkiewicz, M. Becker, M. Rothhardt, H. Bartelt, P. Mergo, L.R. Jaroszewicz, T. Nasilowski, Fiber Bragg gratings in hole-assisted multicore fiber for space division multiplexing, Opt. Lett. 39 (2014) 3571–3574.
[15] N.A. Mohammed, T.A. Ali, M.H. Aly, Performance optimization of apodized FBG-based temperature sensors in single and quasi-distributed DWDM systems with new and different apodization profiles, AIP Adv. 3 (2013), 122125.
[16] T. Ali, M. Shehata, N.A. Mohammed, Design and performance investigation of a highly accurate apodized fiber Bragg grating-based strain sensor in single and quasi-distributed systems, Appl. Opt. 54 (2015) 5243–5251.
[17] N.A. Mohmammed, H.O. Elserafy, Ultra-sensitive quasi-distributed temperature sensor based on an apodized fiber Bragg grating, Appl. Opt. 57 (2018) 5243–5251.
[18] H. Wen, M. Terrel, S. Fan, M. Digonnet, Sensing with slow light in fiber Bragg gratings, IEEE Sens. J. 12 (2012) 156–163.
[19] G. Skolianos, M. Bernier, R. Vallée, M.J.F. Digonnet, Observation of~20 ns group delay in a low-loss apodized fiber Bragg grating, Opt. Lett. 39 (2014) 3978–3981.
[20] Q. Wang, M. Guo, Y. Zhao, A sensitivity enhanced microdisplacement sensing method improved using slow light in fiber Bragg grating, IEEETrans. Inst. Meas. Control. 66 (2017) 122–130.
[21] G. Skolianos, A. Arora, M. Bernier, M. Digonnet, Measuring attostrains in a slow-light fiber Bragg grating, Proc. SPIE. Int. Soc. Opt. Eng. 9763 (2016) 1–10.
[22] M. Pisco, A. Ricciardi, S. Campopiano, C. Caucheteur, P. Mégret, A. Cutolo, A. Cusano, Fast and slow light in optical fibers through tilted fiber Bragg gratings, Opt. Express 17 (2009) 23502–23510.
[23] Q. Wang, P. Wang, C. Du, J. Li, H. Hu, Y. Zhao, Theoretical investigation and optimization of fiber grating based slow light, Opt. Commun. 395 (2017) 201–206.
[24] A. Arora, M. Esmaeelpour, M. Bernier, M.J.F. Digonnet, High-resolution slow-light fiber Bragg grating temperature sensor with phase-sensitive detection, Opt. Lett. 23 (2018) 3337–3340.
[25] H. Wen, G. Skolianos, S. Fan, M. Bernier, R. Vallée, M.J.F. Digonnet, Slow-light fiber-Bragg-grating strain sensor with a 280-femtostrain/√Hz resolution, J. Lightwave Technol. 31 (2013) 1804–1808.

[26] K.M. Dwivedi, G. Trivedi, S. Khijwania, Theoretical analysis of fiber Bragg grating employing novel apodization profile, IEEE Photon. Conf. (2018) 1–2.
[27] T. Erdogan, Fiber grating spectra, J. Lightwave Technol. 15 (1997) 1277–1294.
[28] G. Agrawal, Fiber Gratings (Eds.), Applications of Nonlinear Fiber Optics, 2nd ed., Academic press, 2008, 1–53.
[29] M. Yamada, K. Sakuda, Analysis of almost-periodic distributed feedback slab waveguides via a fundamental matrix approach, Appl. Opt. 26 (1987) 3474–3478.
[30] N.B. Ali, J. Zaghdoudi, M. Kanzari, R. Kuszelewicz, The slowing of light in one-dimensional hybrid periodic and non-periodic photonic crystals, J. Opt. 12 (2010) 1–9.